Q. J. R. Meteorol. Soc. (1999), **125**, pp. 1209–1229

Thermodynamic characteristics of air flowing into and out of precipitating convection over the west Pacific warm pool

By DAVID E. KINGSMILL* and ROBERT A. HOUZE Jr
University of Washington, USA

(Received 30 July 1997; revised 26 June 1998)

SUMMARY

Aircraft data from the Tropical Ocean/Global Atmosphere Coupled Ocean–Atmosphere Response Experiment (TOGA-COARE) indicate the validity of current conceptual models used in cumulus parametrization theories. This study makes use of 1 s (~ 100 m) measurements of temperature, dew-point temperature and pressure taken along the aircraft flight tracks and airborne radar data. The radar data are used to determine the location, depth and horizontal extent of the convection and to categorize the thermodynamic data according to whether the measurements were obtained in precipitation areas or in regions of inflow to convection.

Inflow regions had the highest values of equivalent potential temperature (θ_e), both in the boundary layer and lower free atmosphere, where the convection was deepest and most horizontally extensive, implying a relationship of θ_e to both the depth and breadth of convection. The observations suggest that the thickness of the layer of high-θ_e air may determine the sustainability and, therefore, the horizontal extent of warm-pool convection. The spectrum of values of θ_e in the boundary layer of inflow regions was broad, indicating that the field of θ_e was highly non-uniform at the 1 s (~ 100 m) scale sampled by the aircraft.

The boundary-layer air in precipitating regions also exhibited a broad spectrum of θ_e values, indicating the presence of both outflow from downdraughts and a significant amount of air with characteristics similar to inflow regions. The lowest values in the distribution were about 345 K, suggesting that air parcels transported down into the boundary layer originated from no higher than about 1500 m, or that they underwent substantial mixing.

KEYWORDS: Aircraft observations TOGA-COARE Tropical convection

1. INTRODUCTION

Convective clouds over tropical oceans occur in an environment that is nearly moist adiabatic above the boundary layer. This observation has led to the ideas that:

(i) Convective clouds and their environment are in a statistical equilibrium, with the clouds adjusting rapidly to environmental changes (Arakawa and Schubert 1974) and vice versa (Mapes 1997).

(ii) The source of energy for the convective cloud population is the temperature of the sea surface, which determines the equivalent potential temperature (θ_e) of the parcels of air rising out of the atmospheric boundary layer into the clouds (Emanuel *et al.* 1994).

This view of tropical oceanic convection (Fig. 1) focuses on the boundary layer and is attractively simple: parcels of high surface θ_e air rise out of the boundary layer until they are slowed by entrainment (e.g. Raymond and Blyth 1986). They are replaced by downdraughts of lower θ_e spreading into the boundary layer. Fluxes across the ocean–atmosphere interface then raise the boundary-layer θ_e.

This perspective is the basis for a class of parametrizations of the role of convection in the large-scale thermodynamic structure of the tropical atmosphere. While these theories are probably correct to some degree, there appear to be some possibly significant oversimplifications. Tropical oceanic convection is dominated by mesoscale cloud systems of substantial horizontal extent (e.g. Williams and Houze 1987; Mapes and Houze 1993; Chen *et al.* 1996; Laing and Fritsch 1997; Yuter and Houze 1998) and possessing significant mesoscale circulations (Mapes and Houze 1995; Kingsmill and Houze 1999). A significant question is whether the simplified view of Fig. 1 is adequate to represent the role of these horizontally extensive (i.e. mesoscale) precipitating convective cloud systems

* Corresponding author, present affiliation: Atmospheric Sciences Center, Desert Research Institute, 2215 Raggio Parkway, Reno, Nevada 89512-1095, USA. e-mail: davidk@dri.edu

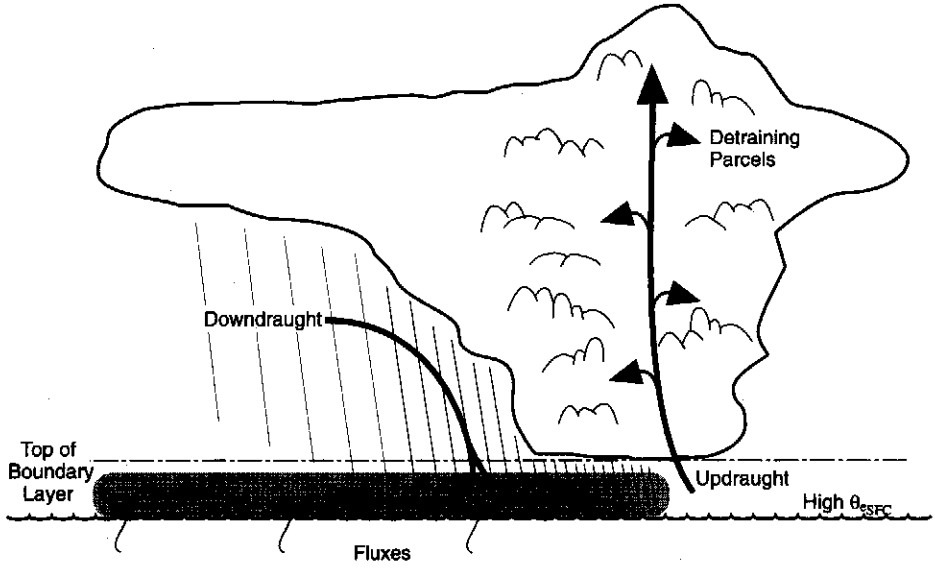

Figure 1. Conceptual model of the processes involved in the statistical equilibrium theory. The wavy line indicates the ocean surface, and the shaded area indicates the region of low equivalent potential temperature, θ_e, transported into the boundary layer by downdraughts. θ_{eSFC} refers to the θ_e of air 10 m or so above the ocean. (Adapted from Emanuel *et al.* 1994).

in the larger-scale circulation. In this paper, we use a combination of airborne radar and flight-level thermodynamic data collected during the Tropical Ocean/Global Atmosphere Coupled Ocean–Atmosphere Response Experiment (TOGA-COARE, Webster and Lukas 1992) to examine the conceptual basis of convective parametrization over tropical oceans, and at the end of the paper we propose several modifications to Fig. 1 as a result of this examination.

2. Data

Details on the TOGA-COARE aircraft observing programme and the specific missions used in our analysis are given in Kingsmill and Houze (1999), hereafter referred to as KH-I. The aircraft performing these missions, two National Oceanic and Atmospheric Administration (NOAA) P-3s and the National Center for Atmospheric Research (NCAR) Electra, are instrumented to make measurements along their flight track (P-3, Jorgensen 1984; Electra: http:/raf.atd.ucar.edu/Bulletins/bulletins.html). The 1 s averaged 'flight level' data consist of several scientific and navigation parameters. For this study, temperature, dew-point temperature, pressure, altitude, horizontal wind speed and direction were the primary variables. Intercomparisons of the measurements obtained when the two aircraft were flying in close formation provided relative calibrations of the sensors (Friehe *et al.* 1996). Inertial Navigation System variables, such as aircraft position and ground speed, were subject to drift errors (Masters and Leise 1993). These errors were corrected by Friehe *et al.* (1996), by incorporating information from the Global Positioning System.

Errors owing to wetting of the temperature and dew-point temperature sensors in cloud or precipitation were addressed in a manner similar to Jorgensen and LeMone (1989). Wetting of the temperature sensor causes it to act somewhat like a wet-bulb thermometer,

and thus it gives readings that are too low. Conversely, wetting of the dew-point temperature sensor causes its mirror to overheat in order to evaporate excess liquid water, and thus it gives readings that are too high.

Corrections to the temperature readings were made by using data from the side-looking CO_2 radiometer on board each aircraft. This instrument can infer air and/or cloud temperature in the immediate vicinity of the aircraft without the biases inherent in the temperature sensor. In cloud or precipitation, the CO_2 radiometer senses the temperature of both the air and the water drops. Under saturated conditions, these temperatures are nearly the same. However, under subsaturated conditions, the wet-bulb temperature of the evaporating water drops is lower than the surrounding air temperature and thus biases the radiometrically inferred temperature downwards, perhaps as much as 1 degC according to Jorgensen and LeMone (1989). Comparisons between data from the CO_2 radiometer and the temperature sensor were made in regions outside of cloud and precipitation throughout each flight, to correct the calibration drift biases that the CO_2 radiometer is known to exhibit. Data in cloud or precipitation were rejected when the aircraft was turning, since the side-looking CO_2 radiometer was sampling either above or below the aircraft flight level.

Biases in dew-point temperature readings are more difficult to correct. If the dew-point temperature exceeded the corrected radiometric temperature, saturation was assumed and the dew-point temperature was set equal to the corrected radiometric temperature value. This assumption could lead to erroneously high values of dew-point temperature in precipitating regions that are characterized by subsaturated conditions.

In a relative sense, the temperature measurements are considered to be more reliable than the dew-point temperature measurements, since the CO_2 radiometer was available for temperature correction whereas there was not an auxiliary water vapour instrument available that could reliably be used to correct dew-point temperature. Quantifying the accuracy of these measurements is difficult. However, we have no reason to believe that our temperature and dew-point temperature measurements are in greater error than previous studies using similar sensors and correction techniques; i.e. errors rarely greater than about 1 degC (e.g. Zipser *et al.* 1981; Jorgensen and LeMone 1989; Jorgensen *et al.* 1997). In addition, the subsaturated precipitating conditions that lead to the greatest errors in these measurements produce biases that partially offset each other from the standpoint of the key variable in our study, θ_e (Bolton 1980).

The thermodynamic data from the 25 aircraft missions examined in this study (see Table 1 of KH-I) were perused in time-series form, and then combined and stratified into categories based on the airborne radar data and/or the environmental wind field. One set of categories stratifies the data into inflow and outflow regions. If in relation to the low-level horizontal winds an aircraft was upstream of actively growing convection and did not encounter precipitation along its track, it was considered to be in a region of inflow unless the θ_e trace indicated large fluctuations (> 4 K) over short time periods (< 120 s). Only the outside-of-precipitation criterion was applied for flights that encountered isolated convection. The sampling area for inflow regions defined this way was sometimes tens of kilometres ahead of the deepest and most active convection.

For the purposes of interpreting the data, regions of precipitation were assumed to be primarily downdraught outflow regions. Tail radar data (from the P-3 aircraft, see KH-I) and microphysical probes (from the Electra aircraft) were used to determine when the aircraft were flying in precipitation, and we determined statistics of the flight-level thermodynamic observations in these rain areas. This criterion excludes data from outflows outside of precipitation, because with a greater amount of boundary layer recovery, the air would be likely to have a distribution of θ_e skewed to higher values compared to outflows within

precipitation. Our stratification technique also does not attempt to identify air parcels being rained into but not descending in downdraughts. However, this simple, objective stratification of the data eliminates the need for using arbitrary thermodynamic thresholds (i.e. using thermodynamic data to threshold itself), which would have otherwise been required (e.g. Barnes and Garstang 1982; Zipser and Caesar 1994). The criterion used for the tail radar data required the existence of a swath of at least 15° above the aircraft of detectable radar echo within a range of 1200 m. A particle concentration exceeding 100 m^{-3}, from either of the Particle Measuring Systems Inc. 2D-C or 2D-P optical array imaging probes, was used as the precipitation criterion for the Electra data.

The lower fuselage (LF, see KH-I) and tail radar data were also used to stratify the thermodynamic data with respect to the horizontal and vertical extent of the convection being sampled. Three spatial categories were defined: shallow convection (S); deep narrow convection (DN); and deep broad convection (DB). S was less than 10 km deep and the largest element of precipitation extended horizontally no more than 30 000 km^2. Most of these systems were less than 5 km deep and had precipitation areas of 100–400 km^2. The S systems documented by aircraft were almost always located within suppressed large-scale regimes. Although shallow convection always accompanied deep convection, when the latter was present it tended to receive the exclusive attention of the aircraft. DN extended more than 10 km in the vertical but was still limited in its horizontal extent ($< 30\,000$ km^2), while DB extended more than 10 km in the vertical but was of larger horizontal extent ($> 30\,000$ km^2). The DN and DB systems were usually sampled within an active large-scale regime. The aircraft did not sample convection that was both shallow and broad. A listing of the stratification of these convective size categories by aircraft mission is given in Table 3 of KH-I.

At least one aircraft usually sampled the lowest 5–8 km of the atmosphere during a mission. The sampling typically consisted of an initial descent from mid-levels (5–8 km) to the boundary layer (20–350 m), followed by a combination of level flight legs interspersed by short ascents up to, and descents down from, ~ 1 km, and then a final ascent near the end of the flight from the boundary layer up to mid-levels. This flight strategy provided the opportunity to analyse the flight-level data in two different ways.

(i) Mean aircraft soundings were constructed from the ascents and descents of the aircraft. The ground- and ship-based balloon soundings nearest in space and time to the precipitation system under study were averaged and appended to the top of the mean aircraft sounding, to extend the sounding to the top of the troposphere.

(ii) Data samples obtained on horizontal flight legs were analysed statistically to determine the typical thermodynamic properties of the boundary layer, and their horizontal variability. For most of the dataset, the two flight altitudes used most frequently were 30 and 150 m. However, during the sampling of DB precipitating regions, the two most common flight altitudes were 150 and 300 m.

3. Stratification of the data

The kinematic characteristics of inflows and outflows of COARE provide a framework within which to view the observed thermodynamic characteristics of the inflows and outflows. We stratify the thermodynamic data according to whether they were obtained in convective inflows or outflows, and in S, DN or DB areas, as defined in section 2. Three important details regarding the application of these categories are: (i) the sampling area for inflow regions was sometimes several tens of kilometres ahead of the radar-observed inflow structures associated with updraught–downdraught interfaces (KH-I); (ii) the size

category with the deepest and most areally extensive precipitation was used for those missions that sampled more than one Mesoscale Precipitation Feature (MPF); (iii) both vertical profiles and horizontal boundary-layer flight legs are examined in this analysis. Of the 25 aircraft missions, 19 contributed to the vertical-profile analysis and 21 to the boundary-layer analysis. The other missions either had instrumentation problems or sampling deficiencies.

4. Vertical profiles of thermodynamic data in convective inflow regions

The vertical profiles of thermodynamic data in this study were mostly for inflow regions, since the aircraft executed relatively few ascents or descents while flying through precipitation. Figure 2 shows mean soundings stratified according to convective category. Below 500 mb the soundings exhibit a conditionally unstable temperature profile, while above 500 mb the temperature profile is near neutral. To illustrate more clearly the layer of conditional instability, Fig. 3 shows the profiles of saturated equivalent potential temperature (θ_{es}) for the three convective categories. The standard, pseudo-adiabatic convective available potential energy (CAPE)* for cloud systems in the S, DN and DB categories was 1738, 1703 and 1954 J kg^{-1}, respectively (Table 1). Enhanced low-level moisture appears to be the main factor accounting for the higher CAPE of the DB sounding. Reversible

* Virtual buoyancy was not used in this calculation.

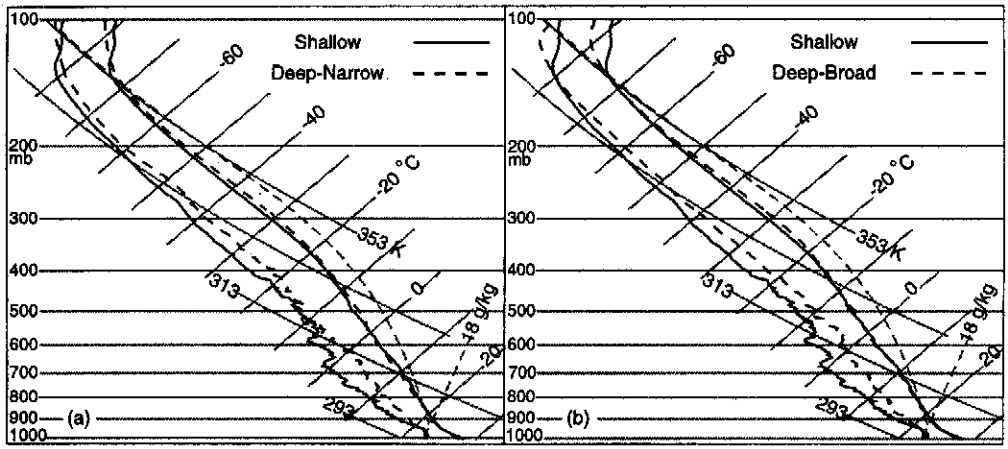

Figure 2. Skew T-log P diagrams of temperature and dew-point for the shallow, deep–narrow and deep–broad composite soundings (see text for definitions). In (a) the shallow sounding (solid lines) is plotted with the deep–narrow sounding (dashed lines) while in (b) the shallow sounding (solid lines) is plotted with the deep–broad sounding (dashed lines).

TABLE 1. Pseudo-adiabatic and reversible CAPE, LFC and CIN for the S, DN and DB composite soundings

Convection category	Pseudo-adiabatic CAPE (J kg^{-1})	Reversible CAPE (J kg^{-1})	LFC (m)	CIN (J kg^{-1})
S	1738	204	1450	−6
DN	1703	192	1150	−8
DB	1954	312	950	−5

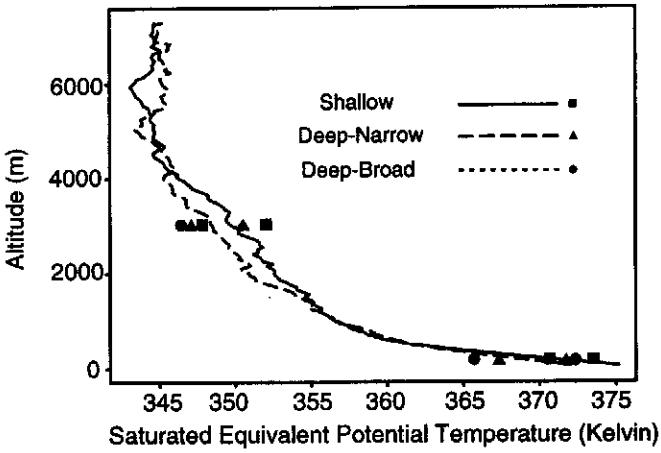

Figure 3. Vertical profiles of saturated equivalent potential temperature for the shallow, deep–narrow and deep–broad composite soundings (see text) of aircraft data obtained by on-board instruments during ascents and descents of the aircraft in the inflow regions of convection over the warm pool. 95% confidence limits at 150 and 3000 m are indicated by squares, triangles and circles.

CAPE values ranged from 192 to 312 J kg^{-1}, a contrast to the near-zero values observed throughout the tropical troposphere by Betts (1982) and Xu and Emanuel (1989). The level of free convection (LFC) exhibits a monotonic decrease in going from the S to DN to DB soundings, in association with increasing values of mixing ratio at low levels. Similar to LeMone *et al.* (1998), Convective Inhibition (CIN), the energetic barrier that parcels must overcome to reach the LFC, is relatively small in all of the soundings and, unlike Raymond (1995), shows no striking tendencies.

The parameters discussed above were derived by using a mean mixing ratio averaged over the lowest 500 m of each sounding. This technique masks the effects of the variability inherent in the low-level moisture profiles. It also discounts the integrated effect of the layer of air parcels that reach their LFC. Figure 4(a) shows the values of CAPE for air parcels originating at the heights indicated by the abscissa. Mapes (1993) defined integrated CAPE (ICAPE) as a mass-weighted sum of CAPE for all low-level air parcels that have positive CAPE. The DB sounding is characterized by the largest ICAPE, since it contains values of CAPE throughout the lowest 1500 m that are generally as large or larger than the other soundings. *This result suggests that a boundary layer with high θ_e throughout its depth, as opposed to a thin surface layer of high-θ_e air, is required in order to sustain deep, broad convection over the warm pool.*

The curves in Fig. 4(b) and (c) reinforce this conclusion. The curves in Fig. 4(b) represent the distance required to lift air parcels to their LFC for the origination heights indicated on the ordinate. In the lowest 500 m, this distance decreases with increasing origination height for the DB sounding, exhibiting a minimum of 600 m for air parcels originating at about 400 m (Fig. 4(b)), while the CIN remains similar to its surface values of about -10 J kg^{-1} (Fig. 4(c)). This means that, not only do DB parcels originating below 400 m have greater CAPE (Fig. 4(a)), but they also reach their LFC sooner (Fig. 4(b)). Above 500 m, the distance required to lift air parcels to their LFC increases rapidly (Fig. 4(b)) and the corresponding values of CAPE and CIN decrease rapidly (Fig. 4(a) and (c)).

The Doppler radar data indicate that the convective updraughts are often fed by a layer of inflow air that is several kilometres deep ($Z_{E_{UI}}$ and $Z_{C_{UI}}$ in Table 4 of KH-I). According to Fig. 4, isolated parcels of air originating above 500 m are not likely to rise to

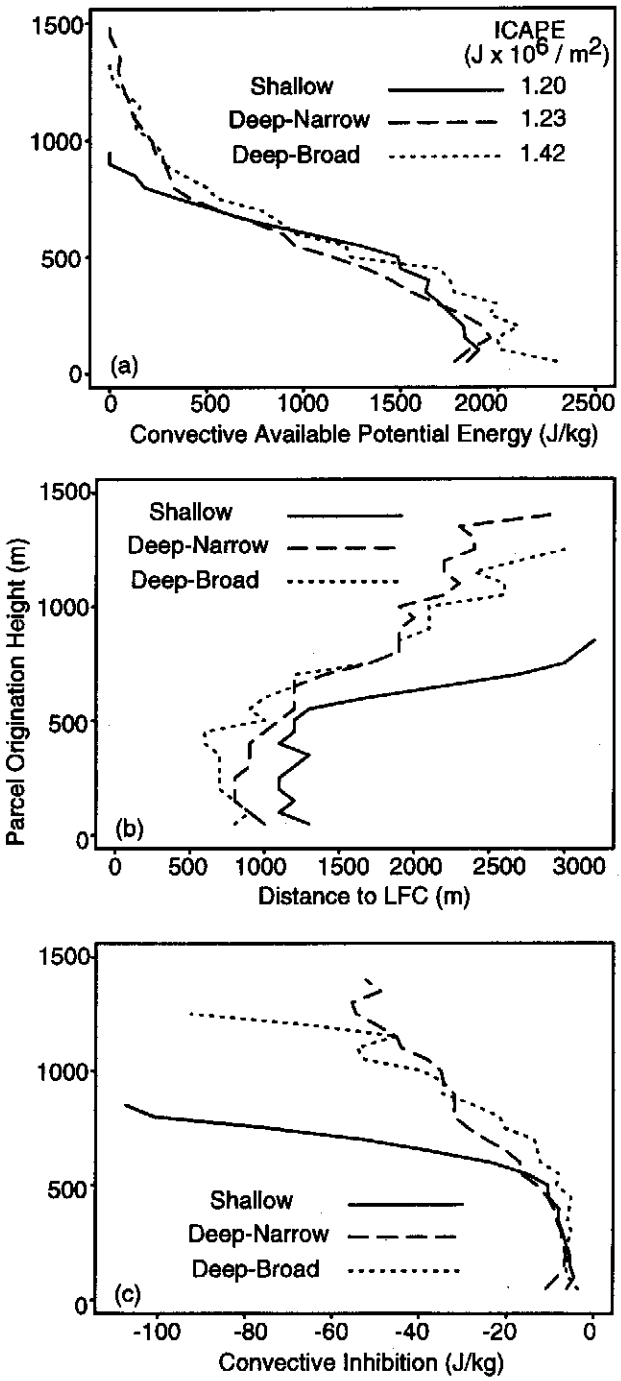

Figure 4. (a) Convective available potential energy (CAPE), (b) distance to the level of free convection (LFC) and (c) convective inhibition (CIN) as a function of parcel origination height for the shallow, deep-narrow and deep-broad composite soundings (see text). Integrated CAPE (ICAPE) values for each sounding are provided in (a).

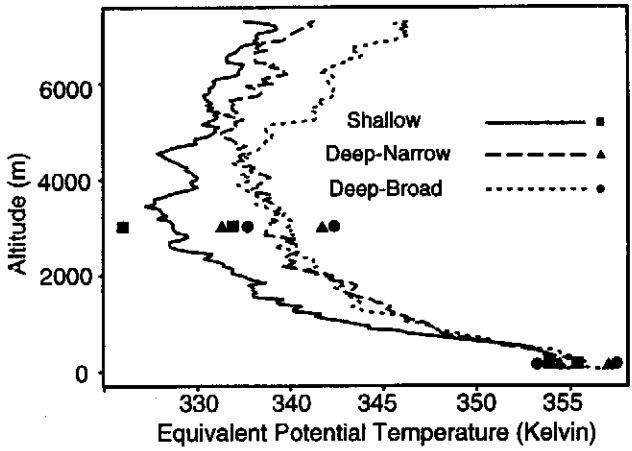

Figure 5. As Fig. 3 but for equivalent potential temperature.

high levels alone. However, since θ_e and θ_{es} decrease with height in the lowest 3 to 4 km (Figs. 3 and 5), the conditions for both potential and conditional instability are in place, and lifting or moistening of a layer of this air would therefore be destabilizing influences. This is relevant because the Doppler radar data show that inflow channels often pass through precipitating regions prior to being lifted by the updraught–downdraught interface (Figs. 6 and 15 in KH-I). Therefore, inflow air may be moistened by evaporating raindrops. If the moistening process culminated in saturation, the air would be able to rise as a layer with near-zero (moist) static stability (i.e. with minimal resistance) when lifted by the updraught–downdraught interface. However, since air at the top of the lifted layer has lower values of θ_e than values at the bottom of the inflow layer, convective overturning would occur within the lifted layer, and the ultimate height to which parcels at the top of the lifted layer rise would probably be below cloud top.

The moisture profile above the boundary layer also varied considerably according to whether convection was S, DN or DB. Profiles of θ_e determined by on-board instruments during ascents and descents of the aircraft illustrate these differences (Fig. 5). Immediately above the boundary layer, the θ_e for the S sounding is less than that of the other soundings. A maximum θ_e difference of about 5 K is evident at the 3–4 km level. Above 4 km, the θ_e for the DN sounding becomes 2 to 4 K lower than that for the DB sounding. *These results indicate that both the depth and breadth of convection over the warm pool was correlated with the humidity of air entering into clouds at low to middle levels.*

Table 2 lists characteristics of the soundings used to construct each of the composites. For the most part, these variables do not correlate with the phase of the intraseasonal oscillation (ISO). However, there is some suggestion of a relationship between the ISO and minimum θ_e, with values > 332 K associated with the active phase and < 332 K with the suppressed phase. A few of the sounding parameters exhibited large anomalies on certain missions. For example, the CIN associated with two of the shallow systems was quite large compared to the others (missions 930201 and 930219). There were also missions with soundings that were characterized by anomalously high or low values of CAPE. For example, there was one DN system with a CAPE of 2756 J kg^{-1} (921102) and another with a CAPE of 1111 J kg^{-1} (921126). These differences appear to be related to low-level values of θ_e. Unlike the variations of θ_e at mid-levels, low-level θ_e exhibits a variability larger than the limits of statistical significance (Fig. 5), which decreases confidence in the

TABLE 2. THERMODYNAMIC CHARACTERISTICS OF THE MEAN AIRCRAFT SOUNDING ASSOCIATED WITH EACH OF THE LISTED MISSIONS

Mission (yy mm dd)	Cat.	Phase of ISO	$\bar{\theta}_{e_{500}}$ (K)	CAPE (J kg^{-1})	CIN (J kg^{-1})	LFC (m)	ICAPE (MJ m^{-2})	$\theta_{e_{min}}$ (K)	$Z_{\theta_{e_{min}}}$ (m)
921102	DN	A	357.8	2756	−6	1050	2.20	329.9	2400
921106	DB	A	353.5	1786	−3	2050	1.59	336.7	4600
921113	S	S	356.1	1958	−3	1100	1.41	326.8	2900
921115	S*	S	354.4	1806	−3	950	1.23	327.8	4600
921119	DB	S	353.9	1772	−4	950	1.42	327.2	5400
921126	DN	S	350.7	1111	−16	1250	0.77	330.2	5100
921128	S	S	353.5	1722	−4	1450	1.41	329.9	3600
921214	DB	A	354.0	1637	−1	800	1.57	335.2	3600
921215	DB	A	356.4	2142	−3	950	1.51	334.5	4200
921216	DN	A	354.9	1683	−10	1150	1.13	338.0	5400
930109	DN	S	355.3	1825	−4	1650	1.47	333.9	4600
930111	S	S*	353.9	1712	−5	1000	1.13	325.9	3100
930116	DN	S	354.6	1509	−7	1300	1.05	332.1	5600
930118	DB	U/A	356.3	1733	−4	850	1.16	337.7	4500
930201	S	U/A	353.9	1856	−40	2550	1.30	328.1	1800
930206	DB	A	352.2	1263	−10	1250	0.93	338.6	2600
930210	DB	A	355.1	2473	−9	1150	1.85	336.1	2500
930219	S	A	352.1	1335	−62	2450	0.77	336.6	2200
930222	DB	A	354.2	1706	−15	1050	1.04	340.6	2500

The convection size category with the deepest and most areally extensive precipitation was used for those missions that sampled more than one MPF. The size category and phases of the ISO are defined as in Table 3 of KH-I together with the assumtpions made where values are marked with an asterisk.

observed trends in CAPE, ICAPE, LFC and CIN (Figs. 2 and 4). This suggests that the boundary layer should be examined more closely.

5. EQUIVALENT POTENTIAL TEMPERATURE IN THE BOUNDARY LAYER

(a) *Average values and the distribution*

The aircraft collected vast amounts of data while flying in the boundary layer at nearly constant altitude. This analysis incorporates almost 220 000 one-second measurements in the altitude range 20–350 m, equivalent to more than sixty flight hours (or about 26 000 km of flight track). Table 3 lists averages and standard deviations of virtual potential temperature, θ_v, and θ_e for each of the missions included in the analysis. Values are stratified into inflow and precipitating regions; precipitating regions for the S category were not sampled.

Precipitating regions were characterized by lower mission means and higher mission standard deviations of θ_e and θ_v compared to the inflow regions. The mission mean deficit of θ_v in precipitating regions ($\bar{\theta}_{v_{INFLOW}} - \bar{\theta}_{v_{PRECIP}}$) spanned the range from 0.2 K (930206) to 3.0 K (921214). The mean and standard deviation for all the mission means was 1.4 K and ±0.6 K, respectively, indicating a 0.3% to 0.7% excess in air density. Mission mean θ_e deficits ($\bar{\theta}_{e_{INFLOW}} - \bar{\theta}_{e_{PRECIP}}$) varied from 0.1 K (930206) to 7.3 K (921102). The mean and standard deviation for all of the mission means was 3.1 K and ±1.8 K, respectively. It is possible that θ_e and θ_v deficits are biased toward slightly lower values due to the partial recovery of the boundary layer sampled in precipitating regions. There does not appear to be any relationship between boundary-layer θ_v or θ_e and the phase of the ISO in these data samples.

TABLE 3. THERMODYNAMIC CHARACTERISTICS OF THE LEVEL FLIGHT LEG DATA FROM 20–350 M ASSOCIATED WITH EACH OF THE LISTED MISSIONS

Mission	CAT	ISO	$\bar{\theta}_{v_{INFLOW}}$ (K)	$\sigma(\theta_{v_{INFLOW}})$ (K)	$\bar{\theta}_{v_{PRECIP}}$ (K)	$\sigma(\theta_{v_{PRECIP}})$ (K)	$\bar{\theta}_{v_{INFLOW}} - \bar{\theta}_{v_{PRECIP}}$ (K)	$\bar{\theta}_{e_{INFLOW}}$ (K)	$\sigma(\theta_{e_{INFLOW}})$ (K)	$\bar{\theta}_{e_{PRECIP}}$ (K)	$\sigma(\theta_{e_{PRECIP}})$ (K)	$\bar{\theta}_{e_{INFLOW}} - \bar{\theta}_{e_{PRECIP}}$ (K)
921102	DN	A	305.2	0.2	304.0	0.6	1.2	358.4	1.7	351.1	6.4	7.3
921106	DB	A	304.0	0.2	302.7	0.5	1.3	354.2	1.1	351.2	3.0	3.0
921113	S	S	304.6	0.2	NA	NA	NA	355.5	1.0	NA	NA	NA
921115	S*	S	304.4	0.4	NA	NA	NA	354.7	1.4	NA	NA	NA
921119	DB	S	304.1	0.4	303.0	0.8	1.1	355.0	1.4	353.3	3.2	1.7
921126	DN	S	302.8	0.5	301.8	0.8	1.0	351.7	1.9	350.4	2.8	1.3
921128	S	S	304.6	0.1	NA	NA	NA	353.9	0.9	NA	NA	NA
921212	DB	A	304.2	0.1	302.4	0.9	1.7	355.9	1.2	350.7	3.7	5.2
921214	DB	A	305.3	0.2	302.3	0.8	3.0	356.5	1.2	352.6	2.7	3.9
921215	DB	A	305.1	0.2	303.6	1.2	1.4	357.9	1.0	355.7	3.2	2.2
921216	DN	A	304.0	0.5	302.6	0.7	1.4	356.0	1.4	353.6	2.2	2.4
930109	DN	S	304.5	0.2	302.7	1.3	1.8	355.7	1.0	352.5	3.2	3.2
930111	S	S*	304.0	0.1	NA	NA	NA	354.5	1.0	NA	NA	NA
930116	DN	S	304.4	0.2	303.1	0.7	1.3	356.6	1.6	354.4	3.2	2.2
930118	DB	U/A	304.3	0.4	303.0	0.8	1.3	356.2	1.0	354.8	2.4	1.4
930201	S	U/A	304.6	0.2	NA	NA	NA	354.2	1.7	NA	NA	NA
930206	DB	A	303.4	0.1	303.2	0.9	0.2	354.2	1.1	354.1	3.0	0.1
930210	DB	A	304.1	0.1	302.9	0.8	1.2	356.7	1.7	353.1	3.3	3.6
930219	S	A	304.1	0.2	NA	NA	NA	353.5	1.2	NA	NA	NA
930220	DB	A	304.2	0.2	302.0	0.7	2.2	356.8	0.8	352.0	2.3	4.8
930222	DB	A	302.8	0.1	301.6	0.8	1.2	353.8	1.0	349.8	2.5	4.0
Mean			304.2		302.7		1.4	355.3		352.6		3.1
Std. Dev.			0.6		0.6		0.6	1.6		1.7		1.8

The size category and phase of the ISO are defined in section 4. The bottom two rows of the table represent the mean and standard deviation of the relevant column of mission mean values.

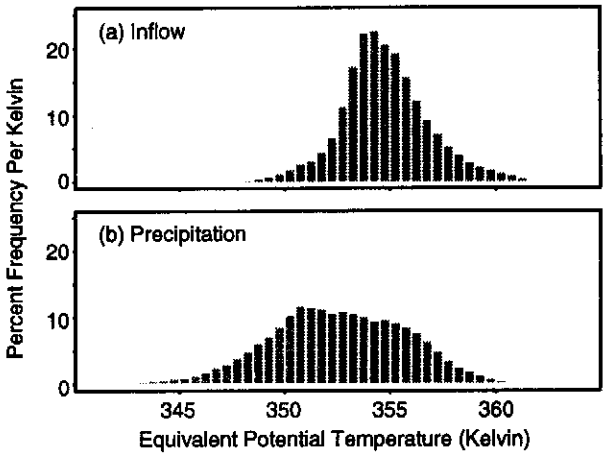

Figure 6. Histograms of boundary-layer equivalent potential temperature stratified into regions of (a) inflow and (b) precipitation.

The mission averages associated with inflow regions (Table 3) are obtained over flight track segments totaling about 100 to 500 km. As such, these values are approximate representations of an average over a grid element in a climate or general-circulation model. From the mean and standard deviation of all the mission means, we infer that the large-scale environment average of θ_e in the inflow region tended to be 355.3 ± 1.6 K, or from ~ 354 to ~ 357 K. These mean values of θ_e in the inflow air are not, however, the values of θ_e of the boundary-layer air parcels rising into the convective clouds. These parcels rising into clouds have a spatial scale $\leqslant 1$ km, and their θ_e values are better indicated by the 1 s samples. In this section, we will examine the probability distribution of the 1 s samples which make up the averages.

This probability distribution is shown in Fig. 6(a), as a histogram of the 1 s values of θ_e observed in inflow regions. Figure 6(b) shows a similar frequency distribution for the 1 s data collected in precipitation regions. Below we first examine the distribution in the inflow regions and then the distribution in the precipitation regions.

(*b*) *Distribution of θ_e in the air flowing into convection*

The histogram of 1 s values of θ_e in convective-inflow regions (Fig. 6(a)) shows that there are numerous parcels of air in the boundary layer with values of θ_e more than one standard deviation higher than the large-scale mean values listed in Table 3. Values of 357–360 K are common. These outliers of the distribution are the only boundary-layer parcels of air capable of reaching the great heights of the maximum cloud tops observed in DN–DB (15–20 km).

The breadth of the distribution of inflow θ_e in Fig. 6(a) indicates important spatial non-uniformity in the boundary layer, much like that observed by Williams *et al.* (1996) for COARE and Nicholls and LeMone (1980) for GATE. This result implies that the mean value of inflow θ_e in Table 3 is not a sufficient indicator of the potential of the boundary layer to support deep convection, which is evidently supported by the outliers of the distribution. It also shows that large-scale grid average values of boundary-layer θ_e are not good predictors of convective-cloud heights.

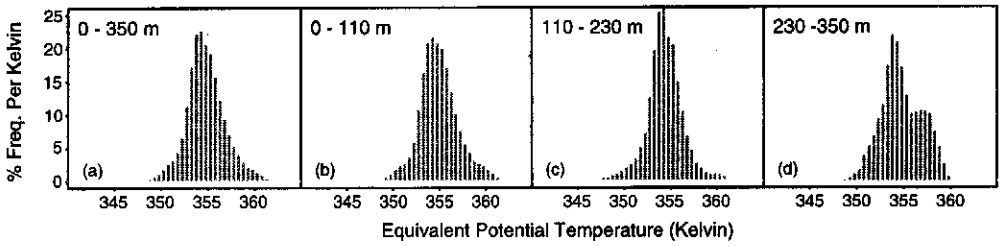

Figure 7. Histograms of boundary-layer equivalent potential temperature for inflow regions stratified into three height regimes: (a) 0–350 m (all altitudes), (b) 0–110 m, (c) 110–230 m and (d) 230–350 m.

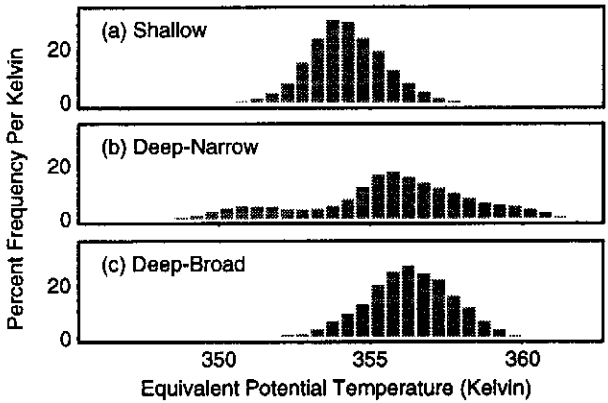

Figure 8. Histograms of boundary-layer equivalent potential temperature for inflow regions stratified by the (a) shallow, (b) deep-narrow and (c) deep-broad convective categories (see text).

Since the aircraft boundary-layer flights were conducted at altitudes ranging from $\sim$ 20 to 350 m, the question arises whether the spread of the distribution in Fig. 6(a) could have been produced by sampling at different levels. Figure 7 stratifies the distribution by altitude. The histograms for the lowest two height regimes (0–110 m, 110–230 m) are almost identical to the histogram spanning the full 0–350 m. The histogram for the upper height regime (230–350 m), while somewhat more complex than the others, is still characterized by a similar dominant mode and overall breadth. These results suggest that sampling at various heights within the boundary layer is not responsible for the broad distributions of θ_e in inflow regions.

Histograms of θ_e in inflow regions are stratified by category of convection in Fig. 8. Progressing from smaller to larger convective systems there is a general increase in the dominant mode of θ_e, resulting primarily from increased moisture. This trend is consistent with the results of the composite aircraft-sounding analysis (Fig. 5) and is a factor contributing to the breadth of the overall inflow histogram (Fig. 6(a)). However, the histograms for each of the convective categories nonetheless exhibit considerable breadth themselves, especially for DN systems where a secondary mode of 351 K is evident. Breaking that histogram up into its constituent parts shows a great deal of mission-to-mission variability (Fig. 9). Each histogram has a different dominant mode. The 351 K secondary mode of inflow θ_e primarily results from the mission on November 26 (921126). The preponderance of low θ_e values observed on this mission may result from a boundary layer still recovering

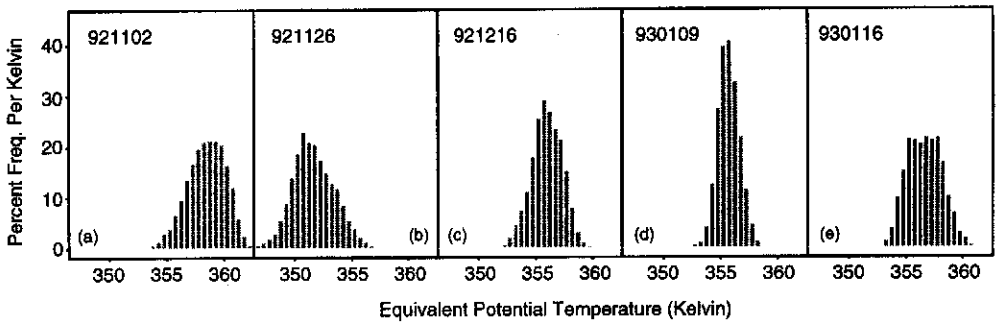

Figure 9. Histograms of boundary-layer equivalent potential temperature for each of the five missions with convection in the deep–narrow category (see text).

from a system that affected the area just hours before aircraft sampling began. Even on this mission, however, there existed parcels of air in the boundary layer with θ_e as high as 357 K, which is consistent with the observed occurrence of some deep convection in this environment. The occurrence of low mean and modal values of θ_e in the inflow evidently does not preclude deep convection, because the distribution almost always contains some parcels capable of deep ascent.

(c) *Distribution of θ_e in precipitating regions*

Since θ_e acts as a conservative tracer (in the absence of diabatic effects), it can be used to estimate the origination height of air parcels transported downward into the boundary layer of precipitating regions, provided we consider the replenishment of boundary-layer θ_e by sensible- and latent-heat fluxes. These fluxes are difficult to quantify by direct observation, which has led to widely varying estimates of boundary-layer recovery time or distance (Parsons *et al.* 1994; Young *et al.* 1995; Jorgensen *et al.* 1997). Therefore, we use the low-valued outliers in the distribution of 1 s samples of θ_e in precipitating regions (Fig. 6(b)) to indicate the boundary-layer air parcels least likely to have been affected by the recovery process. As explained in section 2, the θ_e samples in precipitating regions are taken to represent those areas most likely to have been affected by downdraught outflows. The lowest values in the distribution for precipitating regions are about 345 K. *Together with the profiles of θ_e in Fig. 5, this value of θ_e suggests that air parcels transported down into the boundary layer of precipitating regions either originate from no higher than 1500 m (about 850 mb) or all undergo considerable mixing during descent.* Similar observations have been noted for other tropical environments (Betts 1973, 1976; Barnes and Garstang 1982). This result is, moreover, consistent with the airborne Doppler radar data (section 4(a) of KH-I), which indicate a correspondence between the horizontal winds in downdraught regions and the large-scale winds at 850 mb. However, this inference should be made with caution since pressure-gradient forces may have influenced the large-scale winds during their descent.

Another notable aspect of the histogram of θ_e in Fig. 6(b) is its overall breadth. Evidently, the precipitating regions contained both outflow from downdraughts and a significant amount of boundary-layer air with characteristics similar to inflow regions. Note the considerable overlap between the histograms in Fig. 6(a) and (b). In the light of this result, perhaps it is not surprising that convective cells were often observed with low-level inflow channels originating from and passing through regions of precipitation (section 4(a) of KH-I).

6. Implications for parametrization

Statistical equilibrium of boundary-layer θ_e (Emanuel *et al.* 1994) is premised on a balance among the upward transport of high-θ_e air out of the boundary layer, the downward transport of low-θ_e air into the boundary layer, and the fluxes of sensible- and latent-heat across the ocean–atmosphere interface (Fig. 1). As a cumulus parametrization theory, statistical equilibrium applies best to time-scales greater than 12 h (Emanuel *et al.* 1994); therefore, the mission-oriented aircraft observations are not ideally suited to test its validity. However, the observations do provide information on how components of the statistical-equilibrium theory operate in the context of individual convective systems. In particular, the observations discussed in this paper and in KH-I document the statistics of high-θ_e air transported out of the boundary layer, the lower-θ_e air transported downward to replace it, and the mechanisms through which these transports are accomplished.

(*a*) *Depth and breadth of convection*

The aircraft observations show that the highest values of θ_e in the boundary layer of convective-inflow regions are associated statistically with the deepest and most areally extensive precipitation systems (Fig. 8). DN and DB areas both have numerous outliers of $\theta_e \sim 357$ to 360 K characterizing their regions of inflow. The relationship between high values of θ_e in the boundary layer and deep convection is conceptually straightforward, since non-entraining air parcels with greater buoyant energy rise to greater heights. However, the factors determining the horizontal extent of precipitation are less clear. Yet the horizontally more extensive systems account for a large portion of the vertical mass transport and precipitation over the warm pool, and the factors controlling their occurrence are therefore crucial. Figure 4 suggests that it is the vertically integrated θ_e of the boundary layer (i.e. ICAPE) that determines the horizontal size of deep convective systems over the warm pool. This result is consistent with the results of Yuter and Houze (1998), who by analyzing the joint probability distribution of satellite infrared temperature and aircraft-observed radar echo concluded that the horizontal extent of a precipitation area (radar echo) is controlled by the 'sustainability' of convective cells over a region. They found that a given area of the warm pool can support only a limited number of convective cells at any given time. Since the size of a precipitation area increases as cells weaken and become incorporated into a region of longer lasting stratiform precipitation (Houze 1997), the stratiform area grows as more and more new cells form and decay. The longer that old cells in a region are replaced by new ones, the larger the size attained by the overall (convective plus stratiform) precipitation area. A boundary layer with larger ICAPE should sustain the recurrence of convective cells over a longer time, and therefore produce larger rain areas. We suggest that statistical-equilibrium theories of parametrization could better represent DB over the warm pool by considering the depth of the layer of high-θ_e air (as represented for example by ICAPE) rather than only the surface value. One might argue that the value of θ_e for the lowest layer of a numerical model represents a boundary-layer or surface-layer average; however, as long as that value is set equal to the sea surface temperature, the value is not necessarily representative of the layer average.

A complication in this line of reasoning arises when considering the breadth of the probability distribution of θ_e in the boundary layer of convective-inflow regions. There is a wide range of boundary-layer θ_e values associated with precipitation systems of a given size, and considerable overlap in boundary-layer θ_e between precipitation systems of different sizes (Fig. 8). In contrast, the variations between values of θ_e in the free atmosphere in the environment of different sized precipitation systems appear to be more distinct (Fig. 5). This contrast suggests that the entrainment of dry air into air parcels rising

above the boundary layer, is also an important factor in determining both the vertical- and horizontal-scale of the convection, especially when considering that the airborne Doppler radar observations often showed air flowing into the convection from above the boundary layer (section 4(a) of KH-I). The trend in the θ_e profiles in the three convective categories could partly be a manifestation of differences in the amount of detrainment by prior convection. However, this possibility does not change the fact that the air being entrained into the larger precipitation systems *at the time of the aircraft sampling* contained more moisture than the air being entrained into the smaller precipitation systems.

(*b*) *Initiating and sustaining convection*

Statistical-equilibrium theory does not explicitly address how air parcels are lifted out of the boundary layer. However, this information is vital to understanding the manner in which the CAPE is released. The problem may be divided into two parts: initiating convection in a region devoid of convective clouds and then sustaining convection in a region once initiation has taken place.

This paper focuses on clouds already precipitating. The kinematic structure of these clouds (KH-I) suggests that an ensemble of such clouds is largely self-sustaining over the warm pool. The airborne Doppler radar observations showing sloping updraught–downdraught interfaces suggest that the subsiding denser downdraught air provided the dominant lifting mechanism once precipitating deep convection was established (KH-I, section 4). The updraught–downdraught interfaces were evidently key factors in sustaining the convection. Such a result is consistent with many previous conceptual and modelling studies (e.g. Ludlam 1963; Newton 1963; Thorpe *et al.* 1982; Rotunno *et al.* 1988). As noted above (section 6(a)) the effectiveness of the processes sustaining a mesoscale precipitating cloud system over the warm pool determines the horizontal-scale of the total area covered by precipitating convection. As described in KH-I, the mid-level inflows entering stratiform regions were of very large horizontal-scale, pervading the storm and joining with convective-cell downdraughts by lifting a layer of lower-tropospheric air up at the leading interface of the downdraught. The large horizontal-scale of the subsiding mid-level inflow may be a likely factor in establishing the horizontal-scale of the precipitation system.

It was not possible to determine if the downdraught-outflow structures were also responsible for the initiation of the convection. However, gust fronts, emanating from downdraught outflows have long lifetimes, during which they can separate from their parent clouds and move far away, sometimes into cloud-free areas (Purdom 1976; Wakimoto 1982). When the boundary-layer convergence line comprised of one of these old outflows moves into a cloud-free area, it may trigger new convection, which may in turn lead to a new self-sustaining region of precipitating convection. It is, indeed, not clear that any other mechanism exists for initiating an ensemble of precipitating convection over the warm pool. If this is the case, the occurrence or non-occurrence of precipitating convection in a region with high-θ_e air in the boundary layer is subject to the randomness of pre-existing convection in some other region. That is, a favourable boundary layer is sensitive to rather unpredictable initial conditions—a prescription for chaos, and this raises doubts as to whether parametrization is even a valid concept.

(*c*) *Inhomogeneity of the boundary layer and the nature of downdraughts*

The broad frequency distribution of boundary-layer θ_e air within precipitation, and its overlap with the frequency distribution of boundary-layer θ_e in convective inflow regions (Fig. 6), suggest that only a fraction of all the boundary-layer air in a region of precipitation at any given time had been modified by downdraughts. Since the lowest boundary-layer

values of θ_e in precipitation areas, those least likely to have been affected by the recovery process, were $\sim$ 343 to 345 K (Fig. 6(b)), it appears from Fig. 5 that downdraughts either originated from rather low levels (1–2 km) or were diluted by mixing if they originated from mid-levels.

The Doppler radar observations examined in KH-I indicate that mid-level subsiding inflows were extensive. They constituted long, sloping pathways of downward transport in a deep layer (5–10 km). Figure 5 indicates that the air in the mid-level inflows had θ_e values of 330–340 K. The mid-level inflows co-exist with and appear to have the same time scale as the stratiform precipitation areas. However, the minimum values of θ_e of $\sim$ 343 to 345 K in the boundary layer in precipitation regions (Fig. 6(b)) indicate that the mid-level inflow air did not sink down into the boundary layer—at least not without undergoing considerable mixing and dilution. The radial velocity cross-sections analysed in KH-I suggest that sometimes the mid-level inflows penetrated into regions of active convective cells and merged with convective downdraughts. However, the thermodynamic data in Fig. 6(b) suggest that this low-θ_e air did not reach the boundary layer, or that it was highly modified by mixing with lower-level air by the time it did. Thus, the robust, widespread, and consistently present mid-level inflows described in KH-I seem to have difficulty penetrating to the sea surface (except where they connect with convective-cell downdraughts, as described in KH-I), a result that is consistent with Zipser's (1977) study of a Caribbean squall system.

(*d*) *Revisions of the conceptual model*

The results of this study suggest that the concept of statistical-equilibrium theory, as envisioned by Emanuel *et al.* (1994) and presented in Fig. 1, may be incomplete in some respects. We present a revised version in Fig. 10. At first glance, it appears to be similar to Fig. 1, which simply means that to a first approximation, the Emanuel *et al.* model is consistent with the data of this study. The differences are in the details, and these may be significant.

The first difference is that Fig. 10 acknowledges the wide variation of horizontal-scale. The Emanuel *et al.* version of the conceptual model (Fig. 1) does not address the horizontal-scale of the convection. The precipitation areas of convective systems over the warm pool range from tens to hundreds of kilometres in horizontal dimension. Since the vertical mass transport is proportional, more or less, to the squares of these numbers, it is apparent that the magnitude of convective transport is largely a matter of the breadth of the convective systems. We suggest that parametrization theories address the factors that govern this horizontal-scale. In Fig. 10, we therefore emphasize the value of θ_e averaged over the vertical depth of the boundary layer, in contrast to Fig. 1 which emphasizes the value of θ_e at the surface. In Fig. 7(a) we suggested that the vertical average of θ_e in the boundary layer may control the sustainability and hence the horizontal-scale of the deep convection.

Figure 10 explicitly shows an updraught–downdraught interface, whereas Fig. 1 does not indicate the mechanism by which buoyant air rises up through the free atmosphere. This detail may or may not be important to the parametrization of convection, which does not represent the convective processes explicitly. The updraught–downdraught interface is a well established storm feature (e.g. Ludlam 1963; Newton 1963; Thorpe *et al.* 1982; Rotunno *et al.* 1988) and was such a highly repeatable part of precipitating convection in COARE (KH-I), that we suggest it might be useful as a constraint to any conceptual picture of the convective-overturning process.

More important to the formulation of a parametrization is the layer of inflow air rising over the downdraught outflow. As reported in KH-I, this layer typically exceeded

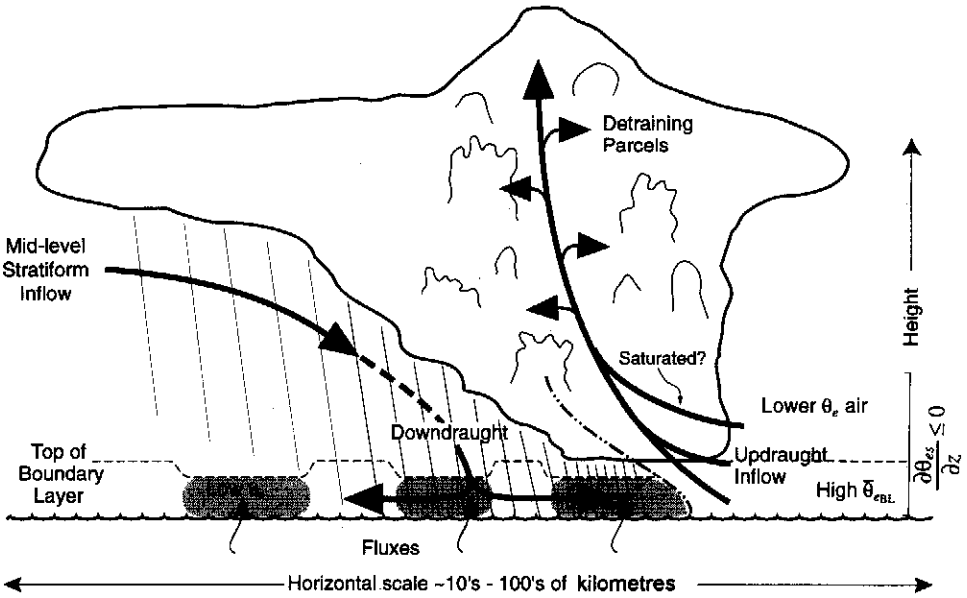

Figure 10. Revision of the conceptual model shown in Fig. 1. Revisions are based upon the results of this study, Kingsmill and Houze (1999), and several GATE studies. Differences from Fig. 1 include the following. (1) An updraught–downdraught interface, indicated by the dash-dot-dot line, which was always present in the convective cells observed by aircraft. (2) Rising air from a layer that is deeper than the planetary boundary layer. (3) Saturated equivalent potential temperature, θ_{es}, decreasing with height in the updraught-inflow layer. In order for the air in the upper portion of the inflow layer to rise it must become moistened after entering the mesoscale convective systems and before the layer is lifted over the downdraught outflow. (4) A vertically averaged value of equivalent potential temperature, θ_e, in the boundary layer ($\bar{\theta}_{e_{BL}}$) rather than the surface value of θ_e ($\theta_{e_{SFC}}$). The degree to which $\bar{\theta}_{e_{BL}}$ is high appears to be related to the sustainability and horizontal extent of the mesoscale convective system. (5) A mid-level inflow to the stratiform region, which has very low θ_e and an uncertain connection to the convective-scale downdraughts. The dashed line indicates this uncertainty. (6) Patches of low θ_e air in the boundary layer of precipitating regions (shaded) rather than a uniformly low value of θ_e. The depth of the boundary layer in low-θ_e areas is assumed to be ~ 200 m lower than the undisturbed boundary layer based on results from GATE.

the depth of the boundary layer. Zipser *et al.* (1981) and Jorgensen *et al.* (1991) have also observed deep inflows in tropical oceanic convection. The TOGA-COARE aircraft show this behaviour consistently throughout a whole season of convection. Figure 1 idealizes the convection as a simple boundary-layer exchange process, in which parcels of air rise from the boundary layer into the free atmosphere in exchange for parcels of downdraught air of lower θ_e sinking into the boundary layer from the free atmosphere. In contrast to this idealization, the Doppler velocity cross-sections, analysed in KH-I, consistently indicated thick layers of air sloping up over a downdraught outflow. The upper part of the layer lay above the boundary layer, as shown in Fig. 10. According to Fig. 5, the θ_e of this air was low. Zipser (1977) suggested that low-θ_e inflow to the convective region of a squall line is entrained into convective downdraughts and does not rise in the updraught. This would imply that the lower θ_e air at the top of the inflow layer did not rise, as shown in Fig. 10, but rather sank (as indicated in Zipser's 1977 Fig. 13). Thus, the Doppler data examined in KH-I do not indicate the existence of Zipser's 'crossover zone' in the preponderance of large mesoscale convective systems sampled by aircraft in COARE. The lower-tropospheric air flowing into the convective-updraught zone was conditionally unstable below about 700 mb, and conditionally neutral-to-unstable up to the 500 mb level (Fig. 3). In addition, the inflow layers observed in the Doppler radar data often passed

through regions of precipitation (Figs. 6 and 15 of KH-I). Therefore, it is possible that the layer of inflow air entered the precipitating region and became moistened by raindrops evaporating into it, and then rose with minimal resistance up over the downdraught outflow.

In the downdraught region of Fig. 10, we indicate an uncertain connection between the subsiding layer of mid-level inflow and the convective-region downdraught (dashed line). As noted in section 6(c), the mid-level inflows have trouble penetrating to the sea surface. Sometimes they appear not to connect to the low-level convective downdraught at all. If a mid-level inflow does merge with a convective downdraught, the low-θ_e air does not reach the boundary layer unmodified. The lowest values of θ_e in the boundary layer equate to the ambient values at the 1 to 2 km level.

The air in the boundary layer of precipitating regions is patchy; some parcels of air have low values of θ_e, while others have values of θ_e no different from the undisturbed boundary-layer air flowing into the updraughts of the storm. We therefore sketch the boundary layer as a region of convective-scale patches of low-θ_e air (shaded in Fig. 10) interspersed among patches of undisturbed boundary-layer air. Although the depth of the disturbed boundary layer was not measured in this study, we indicate a ~ 200 m decrease of the boundary-layer depth for each patch of low-θ_e air; this is based on results obtained during GATE* by Mandics and Hall (1976), Gaynor and Ropelewski (1979), and Fitzjarrald and Garstang (1981). This patchiness of the boundary layer of the precipitating region differs from the simplified conceptual model in Fig. 1, which implies a wholesale replacement of the undisturbed boundary layer with low-θ_e downdraught air. The data suggest that a parametrization scheme should consider what fraction of the boundary layer is replaced by the downdraughts in any given event of convective overturning.

7. Conclusions

Thermodynamic measurements made along the flight tracks of the NOAA WP-3D and NCAR Electra aircraft during TOGA-COARE provide new insights into the vertical exchange of moist static energy (or θ_e) between the atmospheric boundary layer and free atmosphere over the western tropical Pacific Ocean. The exchange is dominated by convection that is both deep and broad, with precipitation areas covering contiguous areas hundreds of kilometres in the horizontal. The DB systems appear to be those sustained over long periods of time when the boundary layer has high-θ_e air distributed through the depth of the boundary layer, not just a thin layer of warm, moist air at the ocean surface.

The 1 s (100 m) flight-track samples of θ_e in the boundary layer indicate a high degree of non-uniformity in the thermodynamics of the air flowing into convective regions. High values of θ_e (e.g. > 357 K) occurred, but they were the outliers of the distribution (Fig. 6(a)). The modal values were lower (354–355 K), and the notion of a uniform boundary layer over a mesoscale or synoptic-scale grid area is not valid.

The analysis of Doppler radar data in KH-I indicates that the vertical exchange of θ_e in observed deep convective systems occurred almost exclusively at sloping updraught–downdraught interfaces, and that it is better described as layer lifting than as parcel lifting. The thickness of the layer of air rising up over the downdraught outflow varied, but it was typically one to several kilometres deep and conditionally unstable (θ_{es} decreasing with height, Fig. 3). Parcel theory leads one to believe that the air at the top of the inflow layer becomes incorporated into downdraughts, while only the air at the bottom of the layer rises (e.g. Zipser's 1977 'crossover zone'). Crossover may happen in some cases; e.g. 8 of the 27 convective cells documented in Table 4 of KH-I have layers of rising air $\leqslant 1$ km

* The Atlantic Tropical Experiment of the Global Atmospheric Research Program.

in depth. However, the kinematic data examined in KH-I showed thick layers of air rising over downdraught outflows in the overwhelming majority of cases in TOGA-COARE. The kinematic data from these cases also indicated that the inflow air often passed through regions of precipitation prior to ascending at the updraught–downdraught interface (Figs. 6 and 15 of KH-I). These observations lead us to believe that the conditionally unstable layers of air flowing into the convective regions became moistened when they entered the mesoscale convective system. The layer of conditionally unstable air could then more easily rise over the spreading downdraught air. The layer of lower-tropospheric ambient air flowing into DN and DB systems differed from that flowing into S convection areas in that it was more humid (Fig. 2) and hence needed less moistening for unrestricted ascent.

The lower-θ_e air entering the boundary layer from the free atmosphere via convective downdraughts does not fill the boundary layer uniformly. Rather the frequency distribution of 1 s (100 m) flight-track samples of θ_e in the boundary layer shows that precipitation areas (sometimes thought of as corresponding to downdraught areas) contain a wide range of values of θ_e, including high values characteristic of undisturbed boundary-layer air. The lowest values of θ_e in the distribution, those least likely to have been affected by the recovery process, are $\sim$ 343 to 345 K, indicating that the air in the extensive mid-level inflows (which had much lower values of θ_e) across stratiform regions (described in KH-I) did not reach the surface, at least not without undergoing considerable mixing. The downdraught air reaching the boundary layer appears rather to have been that of convective-cell downdraughts originating only 1–2 km above the surface. The convective nature of the penetrative downdraughts is consistent with the patchiness of the low θ_e values sampled in the boundary-layer flights.

These conclusions lead to some modifications to the conceptual model in Fig. 1, which guides theories of convective parametrization. Figure 10 incorporates these modifications. Attention is paid in this new figure to the horizontal-scale of the deep convection as well as to its vertical-scale. The vertical average value of θ_e is shown in the boundary layer in Fig. 10 to indicate that it is important in determining the horizontal-scale of the convection, whereas Fig. 1 emphasizes the surface value of θ_e. An updraught–downdraught interface is shown in Fig. 10 since all lifting that we have identified in the radar data obtained by TOGA-COARE aircraft occurred at these concentrated, sloping and nearly discontinuous zones of convergence. The air rising in updraughts is indicated to come from a deeper layer than the boundary layer. This lifting process is viewed as layer lifting, with the air in the inflow layer becoming moistened along its trajectory so that it does not sink in downdraughts but rather rises when it encounters the updraught–downdraught interface. The subsiding mid-level inflow air with extremely low θ_e does not reach the boundary layer, at least not unmixed. The dashed line in Fig. 10 indicates that while the mid-level flow tends to join the convective cell downdraught, the latter produces a patchy pattern of low θ_e in the boundary layer.

This revised conceptual model reformulates the idea of parametrization from a simple parcel-based boundary-layer exchange to an overturning process that involves the movement of layers of air upward and downward. The revised conceptual model needs to be tested by numerical modelling. These tests should investigate how layers of initially unsaturated air, deeper than but including the boundary layer, become moistened and rise over the downdraught outflow. They should also investigate the role of layers of subsiding mid-level inflow air in rearranging the θ_e stratification of the mid-troposphere. These tests will address the fundamental science objectives of TOGA-COARE, which are to understand how the high-θ_e values generated by surface mixing over the oceanic warm pool are conveyed to the larger free atmosphere.

ACKNOWLEDGEMENTS

The authors would like to thank Chris Bretherton, Peggy LeMone, Sandra Yuter and Ed Zipser for reviewing this manuscript. Shuyi Chen, J. Michael Fritsch, Brian Mapes, Bradley Smull and Ming-Jen Yang also provided advice and comments during the course of this study. Grace C. Gudmundson edited the manuscript. Shannon O'Donnell performed the data processing tasks, including much of the airborne Doppler radar analysis. Stacy Brodzik and Sandra Yuter provided software engineering expertise. Data were provided by NOAA (John Daugherty), the Atmospheric Technology Division of NCAR (Bob Rilling) and the University of California, Irvine (Carl Friehe, Sean Burns). This research was supported by NOAA Cooperative Agreement NA67RJ0155. This paper is JISAO contribution number 449.

REFERENCES

Arakawa, A. and Schubert, W. 1974 Interaction of a cumulus cloud ensemble with the large-scale environment. *J. Atmos. Sci.*, **31,** 674–701

Barnes, G. M. and Garstang, M. 1982 Subcloud layer energetics of precipitating convection. *Mon. Weather Rev.*, **110,** 102–117

Betts, A. K. 1973 A composite mesoscale cumulonimbus budget. *J. Atmos. Sci.*, **30,** 597–610

1976 The thermodynamic transformation of the tropical subcloud layer by precipitation and downdraughts. *J. Atmos. Sci.*, **33,** 1008–1020

1982 Saturation point analysis of moist convective overturning. *J. Atmos. Sci.*, **39,** 1484–1505

Bolton, D. 1980 The computation of equivalent potential temperature. *Mon. Weather Rev.*, **108,** 1046–1053

Chen, S. S., Houze, R. A. Jr. and Mapes, B. E. 1996 Multiscale variability of deep convection in relation to large-scale circulation in TOGA COARE. *J. Atmos. Sci.*, **53,** 1380–1409

Emanuel, K. A., Neelin, J. D. and Bretherton, C. S. 1994 On large-scale circulations in convecting atmospheres. *Q. J. R. Meteorol. Soc.*, **120,** 1111–1143

Fitzjarrald, D. R. and Garstang, M. 1981 Vertical structure of the tropical boundary layer. *Mon. Weather Rev.*, **109,** 1512–1526

Friehe, C. A., Burns, S. P., Khelif, D. and Song, X. 1996 'Meteorological and flux measurements from the NOAA WP-3D aircraft in TOGA COARE'. J42–J45 in preprints of the 8th conference on air–sea interaction, American Meteorological Society, Boston, USA

Gaynor, J. E. and Ropelewski, C. F. 1979 Analysis of the convectively modified GATE boundary layer using in situ and acoustic sounder data. *Mon. Weather Rev.*, **107,** 985–993

Houze, R. A. Jr. 1997 Stratiform precipitation in regions of convection: A meteorological paradox? *Bull. Am. Meteorol. Soc.*, **78,** 2179–2196

Jorgensen, D. P. 1984 Mesoscale and convective scale characteristics of mature hurricanes. Part I: General observations by research aircraft. *J. Atmos. Sci.*, **41,** 1268–1285

Jorgensen, D. P. and LeMone, M. A. 1989 Vertical velocity characteristics of oceanic convection. *J. Atmos. Sci.*, **46,** 621–640

Jorgensen, D. P., LeMone, M. A. and Jou, B. J.-D. 1991 Precipitation and kinematic structure of an oceanic mesoscale convective system. Part I: Convective line structure. *Mon. Weather Rev.*, **119,** 2608–2637

Jorgensen, D. P., LeMone, M. A. and Trier, S. B. 1997 Structure and evolution of the 22 February 1993 TOGA COARE squall line: Aircraft observations of precipitation, circulation, and surface energy fluxes. *J. Atmos. Sci.*, **54,** 1961–1985

Kingsmill, D. E. and Houze, R. A. Jr. 1999 Kinematic characteristics of air flowing into and out of precipitating convection over the west Pacific warm pool: An airborne Doppler radar survey. *Q. J. R. Meteorol. Soc.*, **125,** 1165–1207

Laing, A. G. and Fritsch, J. M. 1997 The global population of mesoscale convective complexes. *Q. J. R. Meteorol. Soc.*, **123,** 389–405

Lemone, M. A., Zipser, E. J. and Trier, S. B. 1998 The role of environmental shear and CAPE in determining the structure and evolution of mesoscale convective systems during TOGA COARE. *J. Atmos. Sci.*, **55,** 3493–3518

Ludlam, F. H. 1963 Severe local storms: a review. Pp. 1–30 in *Meteorological Monograph*, **5,** American Meteorological Society, Boston, USA

Mandics, P. A. and Hall, F. F. Jr. 1976 Preliminary results from the GATE acoustic echo sounder. *Bull. Am. Meteorol. Soc.*, **57,** 1142–1147

Mapes, B. E. 1993 Gregarious tropical convection. *J. Atmos. Sci.*, **50,** 2026–2037

Mapes, B. E. 1997 Equilibrium versus activation controls on large-scale variations of tropical deep convection. Pp. 321–358 in *The physics and parameterization of moist atmospheric convection*. Ed. R. K. Smith. Kluwer Academic, Dordrecht, The Netherlands

Mapes, B. E. and Houze, R. A. Jr. 1993 Cloud clusters and superclusters over the oceanic warm pool. *Mon. Weather Rev.*, **121,** 1398–1415

1995 Diabatic divergence profiles in western Pacific mesoscale convective systems. *J. Atmos. Sci.*, **52,** 1807–1828

Masters, J. M. and Leise, J. A. 1993 Correction of inertial navigation with Loran C on NOAA's P-3 aircraft. *J. Atmos. Oceanic Technol.*, **10,** 145–154

Newton, C. W. 1963 Dynamics of severe convective storms. Pp. 33–58 in *Meteorological Monograph* **5,** American Meteorological Society, Boston, USA

Nicholls, S. and LeMone, M. A. 1980 The fair-weather boundary layer in GATE: The relationship of subcloud fluxes and structure to the distribution and enhancement of cumulus clouds. *J. Atmos. Sci.*, **37,** 2051–2067

Parsons, D., Dabberdt, W., Cole, H., Hock, T., Martin, C., Barrett, A-L., Miller, E., Spowart, M., Howard, M., Ecklund, W., Carter, D., Gage, K. and Wilson, J. 1994 The Integrated Sounding System: Descriptions and preliminary observations from TOGA COARE. *Bull. Am. Meteorol. Soc.*, **75,** 553–567

Purdom, J. F. W. 1976 Some uses of high-resolution GOES imagery in the mesoscale forecasting of convection and its behavior. *Mon. Weather Rev.*, **104,** 1474–1483

Raymond, D. J. 1995 Regulation of moist convection over the west Pacific warm pool. *J. Atmos. Sci.*, **52,** 3945–3959

Raymond, D. J. and Blyth, A. M. 1986 A stochastic mixing model for nonprecipitating cumulus clouds. *J. Atmos. Sci.*, **43,** 2708–2718

Rotunno, R., Klemp, J. B. and Weisman, M. L. 1988 A theory for strong, long-lived squall lines. *J. Atmos. Sci.*, **45,** 463–485

Thorpe, A. J., Miller, M. J. and Moncrieff, M. W. 1982 Two-dimensional convection in nonconstant shear: a model of mid-latitude squall lines. *Q. J. R. Meteorol. Soc.*, **108,** 739–762

Wakimoto, R. M. 1982 The life cycle of thunderstorm gust fronts as viewed with Doppler radar and rawinsonde data. *Mon. Weather Rev.*, **110,** 1060–1082

Webster, P. J. and Lukas, R. 1992 TOGA COARE: The coupled ocean–atmosphere response experiment. *Bull. Am. Meteorol. Soc.*, **73,** 1377–1416

Williams, M. and Houze, R. A. Jr. 1987 Satellite-observed characteristics of winter monsoon cloud clusters. *Mon. Weather Rev.*, **115,** 505–519

Williams, A. G., Kraus, H. and Hacker, J. M. 1996 Transport processes in the tropical warm pool boundary layer. Part I: Spectral composition of fluxes. *J. Atmos. Sci.*, **53,** 1187–1202

Xu, K-M. and Emanuel, K. E. 1989 Is the tropical atmosphere conditionally unstable? *Mon. Weather Rev.*, **117,** 1471–1479

Young, G. S., Perugini, S. M. and Fairall, C. W. 1995 Convective wakes in the equatorial western Pacific during TOGA. *Mon. Weather Rev.*, **123,** 110–123

Yuter, S. E. and Houze, R. A. Jr. 1998 The natural variability of precipitating clouds over the western Pacific warm pool. *Q. J. R. Meteorol. Soc.*, **124,** 53–99

Zipser, E. J. 1977 Mesoscale and convective-scale downdraughts as distinct components of squall-line circulation. *Mon. Weather Rev.*, **105,** 1568–1589

Zipser, E. J. and Caesar, K-A. L. 1994 'The structure of cold pools produced by mesoscale convective systems during TOGA COARE'. Pp. 29–32 in preprints of the 6th conference on mesoscale processes. American Meteorological Society, Boston, USA

Zipser, E. J., Meitin, R. J. and LeMone, M. A. 1981 Mesoscale motion fields associated with a slowly moving GATE convective band. *J. Atmos. Sci.*, **38,** 1725–1750